THE JOURNAL OF PHYSICAL CHEMISTRY Letters

Letter

pubs.acs.org/JPCL

Electrochemical Supercapacitor Electrodes from Sponge-like Graphene Nanoarchitectures with Ultrahigh Power Density

Zhanwei Xu,[†,‡,§] Zhi Li,*[,†,‡,§] Chris M. B. Holt,[†,‡] Xuehai Tan,[†,‡] Huanlei Wang,[†,‡] Babak Shalchi Amirkhiz,[†,‡] Tyler Stephenson,[†,‡] and David Mitlin*[,†,‡]

[†]Chemical and Materials Engineering, University of Alberta, Edmonton, Alberta T6G 2 V4, Canada

[‡]National Institute for Nanotechnology (NINT), National Research Council of Canada, Edmonton, Alberta T6G 2M9, Canada

Supporting Information

ABSTRACT: We employed a microwave synthesis process of cobalt phthalocyanine molecules templated by acid-functionalized multiwalled carbon nanotubes to create three-dimensional sponge-like graphene nanoarchitectures suited for ionic liquid-based electrochemical capacitor electrodes that operate at very high scan rates. The sequential "bottom-up" molecular synthesis and subsequent carbonization process took less than 20 min to complete. The 3D nanoarchitectures are able to deliver an energy density of 7.1 W·h kg^{-1} even at an extra high power density of 48 000 W kg^{-1}. In addition, the ionic liquid supercapacitor based on this material works very well at room temperature due to its fully opened structures, which is ideal for the high-power energy application requiring more tolerance to temperature variation. Moreover, the structures are stable in both ionic liquids and 1 M H_2SO_4, retaining 90 and 98% capacitance after 10 000 cycles, respectively.

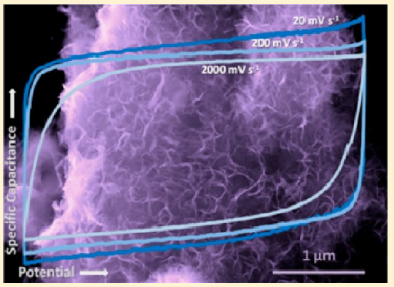

SECTION: Energy Conversion and Storage; Energy and Charge Transport

With increasing power requirements for electric/hybrid vehicles and power back up, supercapacitors have attracted much attention recently due to their ability to supply much higher power density as compared to batteries.[1−4] Graphene and carbon nanotubes (CNTs) are considered as promising materials for the next-generation supercapacitors due to their high specific surface area, excellent electrical conductivity, and high chemical and thermal stability.[1,5−8] Graphene-based electrode materials have been investigated for the application of supercapacitors in aqueous, organic and ionic liquid (IL) electrolytes.[1,9,10] However, due to the strong van der Waals force between neighboring layers, graphene readily packs and forms aggregated structures. This greatly limits electrolyte transfer and ion accessibility, especially in ILs that are more viscious.[11] This, in turn, severely limits the rate capability of the electrodes, forcing them to operate in effect as "mediocre batteries".[12] New materials, such as laser-scribed graphene, curved graphene, and solvated stacking-free graphene, have been created to solve this problem.[2,13,14] One of the promising solutions is to synthesize graphene with three-dimensional (3D) structure.[15−19] Theoretical calculations show that a 3D graphene−CNT network is an ideal structure for high power applications due to the presence of fast electrolyte transfer channels.[15] Following this theoretical work, graphene with 3D structure has been successfully synthesized via chemical vapor deposition,[16,18] the hydrothermal method,[20] and a "breath-figure" technique.[17]

Microwave synthesis is a versatile technique for creation of new materials, offering higher reaction rates, better selectivity, and shorter reaction times as compared to conventional thermal methods.[6,21,22] This technique has recently been used to synthesize graphene.[10,23−25]However, in most cases, the graphene was made using a graphite precursor via "top-down" strategies, where larger graphite particles are chemically and/or physically exfoliated. Metal phthalocyanine (MPc) compounds are conjugated macromolecules. They readily connect to other conjugated materials via $\pi-\pi$ interactions, hydrogen bonding, and coordinate bonding.[26] The MPc molecule ($M_w \approx 600$) is about 2 nm in size.[27,28] Therefore, such molecules are ideally suited for coupling with other nanomaterials, such as with CNTs. In addition, the conversion from MPc to graphene is self-catalyzed by the metal (such as Co) from MPc. The goal of this study is to explore this approach in regard to achieving a graphene-based architecture suited for fast electrolyte transfer. As we will demonstrate, the achieved nanostructures are adapted for fast electrolyte transfer that they allow the electrode to be operated in an IL at room temperature. Normally, supercapacitors based on conventional ILs only perform well at a temperature of 60 °C or higher. This is due to the high viscosity and large ion sizes intrinsic for most ILs that lead to unacceptable diffusional losses at fast scan rates, that is, at high power. It is only with custom-tailored eutectic ILs that lower-temperature performance may be achieved using microporous carbons.[29]

Received: August 17, 2012
Accepted: September 25, 2012
Published: September 25, 2012

Scheme 1 illustrates the synthesis strategy for 3D sponge-like graphene (defined as 3D SPG). Cobalt phthalocyanine (CoPc)

Scheme 1. Diagram of the Synthesis Process of a 3D Nanostructure Constructed by CNT-Supported Graphene

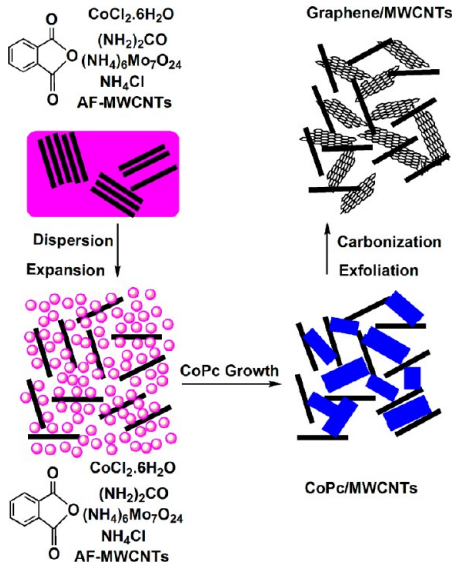

and acid-functionalized multiwalled carbon nanotubes (AF-MWCNTs) were used as the precursors for the 3D SPG. The weight fraction of the nanotubes was ~7.5% in the final SPG product. The CoPc, in turn, was synthesized via microwave heating of the precursor chemicals. AF-MWCNTs were utilized as supports and nucleation sites for CoPc formation. The Co atoms and H atoms of CoPc can form coordination bonds and hydrogen bonds with the O atoms on AF-MWCNTs.[30] Both the CoPc synthesis and in situ carbonization steps were performed in one sequence. The starting materials were microwave-heated at a power of 600 W for 10 min, followed by a 10 min heating at 800 W to create SPG. The postmicrowaved product was immediately quenched using ice water. The quench aided in the exfoliation of the material, transforming it into graphene flakes. This was due to the thermal stress induced by fast quenching from high temperature.[31] Without the quench, the final product was graphite rather than graphene. The AF-MWCNTs are critical for the carbonization process as well as being a "skeleton" in the composites. The CoPc platelets remain templated and therefore dispersed by the AF-MWCNTs during the the carbonization process. Moreover, the gases evolved during the reaction also act as dispersants. NH_3 and HCl gases are generated from the decomposition of NH_4Cl at a sufficiently high temperature (~140 °C) by the following reaction:

$$NH_4Cl(s) \rightarrow NH_3(g) + HCl(g) \quad (1)$$

This results in an expansion force. There is an adsorption between the AF-MWCNTs and NH_3 and HCl molecules, which is accomplished primarily by hydrogen bonding and secondarily by van der Walls force. The hydrogen bond is between the surface O atoms of AF-MWCNTs and the H atoms of NH_3, as well between the N atom of NH_3 and the surface H atoms of AF-MWCNTs. The NH_3 and HCl gases will also locally cover and protect the graphite from oxidation during microwave synthesis,[25] relegating the need for an inert global gas environment inside of the reactor. (Additional details of the synthesis procedure are provided in the Supporting Information). A scanning electron microscopy (SEM) micrograph of the subsequent CoPc−MWCNTs nanocomposites (without carbonization) and the associated X-ray diffraction (XRD) pattern are presented in Figure S2 (Supporting Information). The AF-MWCNT−graphite composites, synthesized as a baseline, are shown in Figure S3 (Supporting Information). X-ray photoelectron spectroscopy (XPS) analysis demonstrates that the obtained 3D SPG primarily consists of C with only a minor amount of N and O heteroatoms (Figure S4, Supporting Information). The atomic percentages of C, N, and O atoms are 95.6, 1.6, and 2.8%, respectively. N atoms possibly originate from the precursor CoPc,[32] and O atoms can be attributed partially to the AF-MWCNTs used as the supports

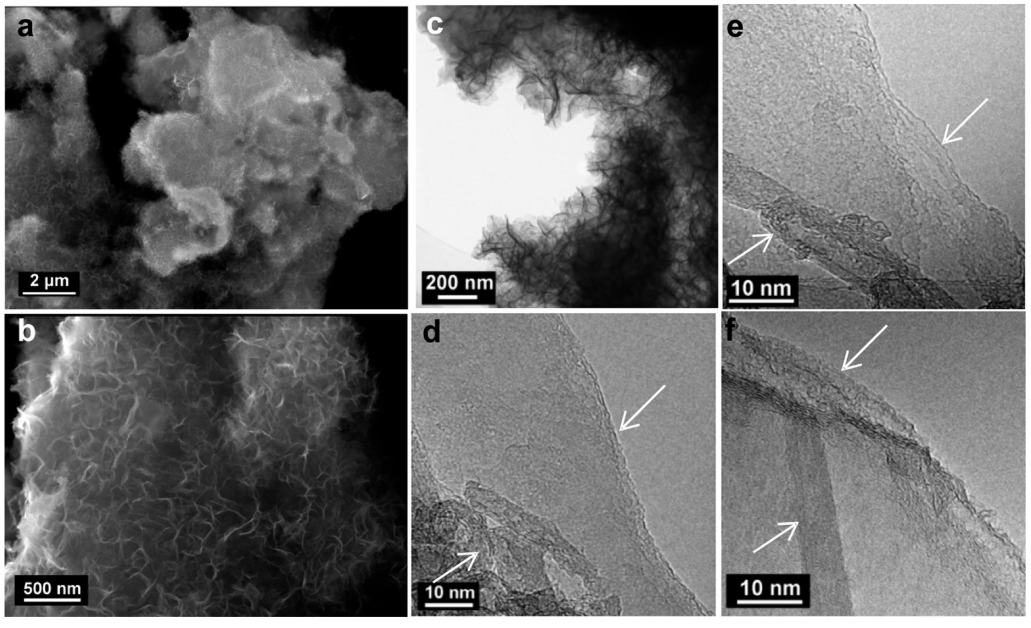

Figure 1. (a,b) SEM micrographs of the 3D SPG. (c) TEM, and (d,e,f) HRTEM micrographs of the 3D SPG.

dx.doi.org/10.1021/jz301207g | J. Phys. Chem. Lett. 2012, 3, 2928−2933

and to a minor amount of graphene oxidation during the quench from high temperature when shielding gas is not present.

Representative SEM micrographs show that the obtained product exhibits a very uniform sponge-like morphology with a 3D macroporous structure (Figure 1a and b). Complementary transmission electron microscopy (TEM) analysis of SPG is shown in Figure 1c–f. Figure 1c shows a low-magnification TEM micrograph of the 3D SPG composite, illustrating its general morphology. The HRTEM micrographs, shown in Figure 1d–f, highlight the typical thickness range observed for the graphene flakes. Figure 1d shows a platelet with five layers. Figure 1e shows a "thin" platelet that is two layers thick, while Figure 1f shows a representative "thick" platelet that is eight layers. The top arrow in each micrograph points to the portion of the graphene flake that was aligned normal to the electron beam allowing for thickness analysis. The bottom arrow in each micrograph highlights the AF-MWCNTs, which are fractured but intact in the final SPG.

Figure 2a shows an asymmetric (002) XRD peak that may be deconvoluted into a peak originating from AF-MWCNTs and a

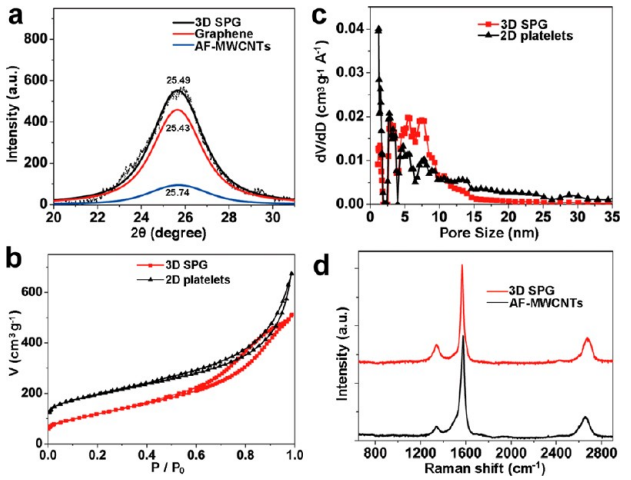

Figure 2. (a) Experimental XRD patterns of 3D SPG and of AF-MWCNTs and the deconvoluted (002) reflection due to graphene. (b) Nitrogen adsorption–desorption isotherms and (c) pore size distribution of the 3D SPG and 2D platelets. (d) Raman spectra of the AF-MWCNTs and 3D SPG.

peak originating from the graphene flakes. The experimentally measured AF-MWCNTs (002) reflection is at $2\theta = 25.74°$ (the entire plot is shown in Figure S5, Supporting Information). By comparing the positions of the (002) AF-MWCNTs with that of the (002) 3D SPG, it can be concluded that the (002) graphene peak is centered at $2\theta = 25.43°$. Additional details of the XRD pattern analysis are shown in the Supporting Information, Figure S5. That suggests that the interlayer distance of the graphene is about 0.35 nm and the graphene nanoplatelets are, on average, five layers thick. The nitrogen adsorption isotherms of the 3D SPG and the reference commercially available 2D graphene platelets are shown in Figure 2b; both of them are type II/IV. The 3D SPG shows more hysteresis in the relative pressure ratio between 0.6 and 0.9, indicating that it contains a higher fraction of mesopores. Moreover, the 3D SPG exhibits significantly higher incremental pore volume for the pores between 4 and 10 nm, confirming its open structure (Figure 2c). According to the *t*-plot method, the amount of microporous surface area of the 3D SPG is almost zero, while that of 2D platelets is about 39%. The measured Brunauer–Emmett–Teller (BET) surface areas of the 3D SPG and of the 2D platelets are 418 and 677 $m^2\ g^{-1}$. The theoretical surface area of single-layer graphene is 2630 $m^2\ g^{-1}$. Thus, BET predicts that the average thickness of the graphene platelets in SPG is 5–6 layers, agreeing well with the HRTEM and XRD analysis. In the control experiments that were prepared without rapid quenching, the graphitic structure is 20 layers thick (shown in the Supporting Information, Figure S6). Raman spectroscopy was employed to further characterize the structure of the 3D SPG. The results are shown in Figure 2d, with 3D SPG being the top plot and the AF-MWCNTs being the bottom. The Raman shift of AF-MWCNT supports shows the D band, G band, and 2D band at 1341, 1578, and 2686 cm^{-1}, respectively. The ratio of D and G band intensity is correlated to the in-plane crystal domain size, which is often used to estimate the degree of disorder in graphite.[33] The intensity ratio I_D/I_G is 0.13, indicating that the AF-MWCNTs used as templates possess high crystallinity. This was supported by TEM analysis (shown in the Supporting Information, Figure S7). The D band and G band of the 3D SPG are in similar positions to those of the AF-MWCNT supports. The SPG also possesses a very low value of I_D/I_G (0.17), indicating that the graphene of SPG has a high degree of crystallinity. The 2D band position of the SPG (~2689 cm^{-1}) supports that the graphene is, on average, about five layers thick. Thermal analysis, shown in Figure S8 (Supporting Information), shows an initial mass loss of 3.1% at about 120 °C, corresponding to the evaporation of physically adsorbed water. The main exothermal peak is at ~520 °C with ~96.5% weight loss in air, agreeing well with known oxidation behavior of graphene.

The highly mesoporous structure of 3D SPG is ideally suited for electrochemical energy storage applications, where one would normally experience diffusional limitations if employing conventional microporous carbons. Thus, one obvious application is for room-temperature operation of a supercapacitor using an IL electrolyte. As described in the introduction, using an IL electrolyte normally necessitates a 60 °C or higher environment. Moreover, the physical connection between the graphene platelets and CNTs offers an excellent electron transfer pathway down the electrode.[34]

The electrodes were tested in 1 M H_2SO_4 and in a commercially available (1-butyl-1-methylpyrrolidinium bis-(trifluoromethylsulfonyl) imide, BMPY TFSI) IL. In a two-electrode (symmetric) cell with a 1 M H_2SO_4 electrolyte, the SPG exhibits a box-like cyclic voltammogram (CV) shape. This is shown in Figure 3a. At sweep rates as high as at 500 mV s^{-1}, the CV curves maintain an almost perfect rectangular shape, indicating good electrical conductivity and fast electrolyte transfer for the electrode. The CVs of the SPG were also recorded in a three-electrode setup, yielding similar results. That data is provided in Figure S9 (Supporting Information). Figure 3b shows the specific capacitance of 3D SPG calculated by galvanostatic charge/discharge cycling at different current densities, with 2D graphene platelets tested as a baseline. At a low current density of 0.1 A g^{-1}, the specific capacitance of the 3D SPG is actually lower than that of 2D platelets. This is expected due the much higher surface area of the 2D platelets (418 versus 677 $m^2\ g^{-1}$). However, at current densities above 8 A g^{-1}, the capacitance of the SPG is actually higher than that of 2D platelets. This can be attributed to the mesoporous versus microporous structures of the electrodes. Figure 3c demon-

dx.doi.org/10.1021/jz301207g | J. Phys. Chem. Lett. 2012, 3, 2928–2933

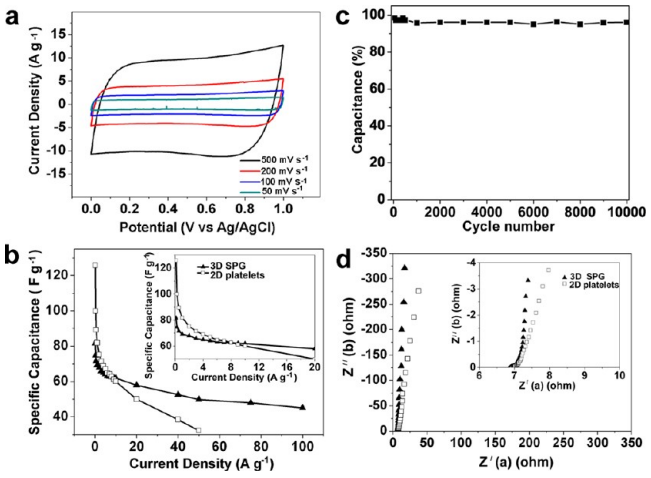

Figure 3. Electrochemical performance of 3D SPG in 1 M H_2SO_4. (a) CV curves of the 3D SPG at various scan rates in a two-electrode system. (b) The specific capacitance of 3D SPG and 2D platelets with respect to the charge/discharge-specific currents. (c) Capacitance retention of 3D SPG versus the cycle number in 1 M H_2SO_4. (d) Nyquist plots of 3D SPG and reference 2D platelets.

strates that in a three-electrode configuration, the 3D SPG electrode shows essentially negligible cycling-induced degradation (less than 2%) even after 10 000 cycles at 1 A g^{-1}. It took approximately 2.3 min to perform one charge−discharge cycle and a total of 16 days to finish the entire cycling study. Figure 3d compares the Nyquist plots for the 3D SPG electrode and for the baseline 2D, in a three-electrode configuration. The transition to ideal capacitive behavior at a higher frequency for the 3D SPG highlights that its macroporosity is advantageous for the fast frequency response.

Tested in the IL at 60 °C, both 3D SPG and 2D platelets show nearly perfect rectangular CVs at 20 and 200 mV s^{-1} (Figure 4a and b). At 2000 mV s^{-1}, the CV for 3D SPG shows much less distortion than that of the 2D platelets (Figure 4c). Very importantly, for a scan rate of 200 mV s^{-1}, the SPG exhibits almost the same performance at 25 versus 60 °C. Conversely, at that sweep rate, the 2D platelets suffer from a severe CV distortion at 25 °C. When tested at 60 °C, even at a very high sweep rate of 2000 mV s^{-1}, the 3D SPG can still achieve around 85% of the maximum capacitance. The sizes of $SO_4^{2-}(H_2O)_{12}$ and H_3O^+ in 1 M H_2SO_4 aqueous solution were reported to be 0.533 and 0.42 nm, respectively.[35] The maximum dimension of the anion and cation in BMPY TFSI are much larger, being 0.79 and 1.1 nm.[36] At 25 °C, it is expected that these ions are relatively slow to diffuse under the action of an applied field. Due to the mesoporous structure of the 3D SPG versus the microporous structure of the 2D platelets, the capacitive performance is less influenced by ion size and ion mobility. In the IL, the normalized specific capacitance of 3D SPG reaches 16.2 μF cm^{-2} at 0.1A g^{-1}, almost double the value of 2D platelets. As observed in aqueous electrolyte, the specific capacitance of 3D SPG fades significantly slower than that of 2D platelets with an increase of current density. It shows a capacitance of 53 F g^{-1} even at 100 A g^{-1}, around 78% of the capacitance at 0.1 A g^{-1} (Figure 4d). As shown in the Ragone plots, the energy density of SPG at a low power density of 75 W kg^{-1} is 21.4 W·h kg^{-1}, higher than that of the 2D platelets (16.7 W·h kg^{-1}) but still not outstanding among the values achieved by carbons with extremely high surface area.[37,38] However, the ability to deliver

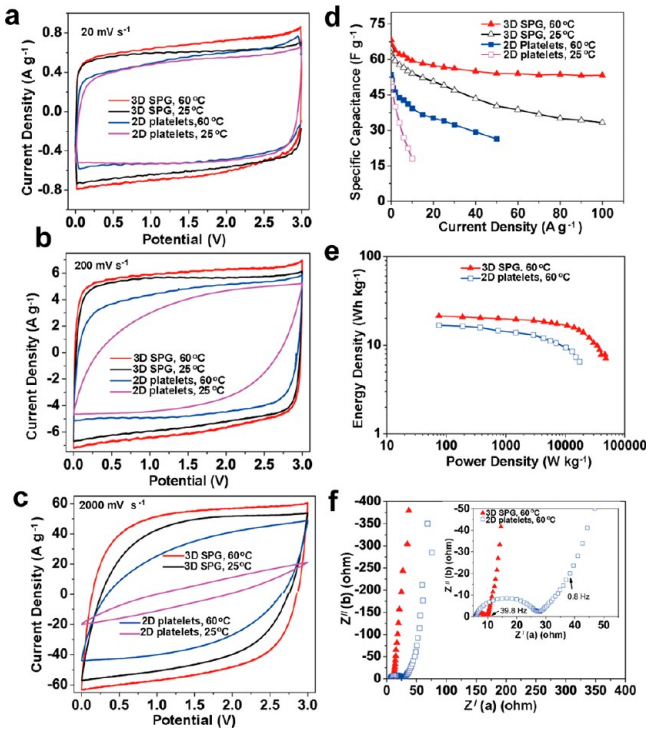

Figure 4. Electrochemical performance of SPG in an IL. (a−c) CV curves of 3D SPG and reference 2D platelets at 20, 200, and 2000 mV s^{-1}. (d) The specific capacitance of 3D SPG and 2D platelets with respect to the charge/discharge-specific currents. (e) Ragone plots of 3D SPG and 2D platelets. (f) Nyquist plots of 3D SPG and reference 2D platelets.

an energy density of 7.1 W·h kg^{-1} at an extra high power density of 48 000 W kg^{-1} is where the 3D SPG really distinguishes itself from other materials (Figure 4e). The SPG also exhibits an excellent cycle life. After 10 000 cycles at 5 A g^{-1} (about 5 days to finish the test), it still keeps 87% of its initial capacitance (Figure S11, Supporting Information).

In both aqueous and IL electrolytes, the 3D SPG shows an attractive advantage over 2D platelets at higher current densities. This performance can be attributed to its unique sponge-like, fully opened, and interconnected structure, which facilitates fast electron and electrolyte transfer. Figure 4f shows the Nyquist plots recorded from 0.025 to 50 000 Hz at an open circuit potential in IL electrolytes. The charge-transfer resistance (estimated by the radius of the semicircle in the high-frequency range) for carbon materials is related to the pore structure.[39] Tortuous pore structure will increase the size of the semicircle. Benefiting from a fully opened structure, the charge-transfer resistance of SPG is about 1/4 of that of 2D platelets. Fast electrolyte transfer in SPG can be confirmed by its shorter Warbug-type line (the 45° portion) than that of the 2D platelets. The "onset" frequency is defined as the highest frequency where the impedance of the electrode starts to be dominated by capacitive behavior (Nyquist plot starts to go vertical). It reflects the highest frequency where most of the capacitance is retained. The onset frequency of 3D SPG is 39.8 Hz, much higher than that of 2D platelets (0.8 Hz), indicating the fast capacitive response of SPG.

In summary, we have fabricated a graphene−CNTs 3D architecture with a unique sponge-like morphology via microwave synthesis and carbonation of CoPc using AF-MWCNT as supports, followed by exfoliation of graphite via

dx.doi.org/10.1021/jz301207g | J. Phys. Chem. Lett. 2012, 3, 2928−2933

thermal stress. The overall process was completed within 20 min. Due to the high conductivity of graphene and the fully accessible surface, the obtained product exhibits attractive energy density, especially at high current densities, for the application of supercapacitors in both aqueous and IL electrolytes.

EXPERIMENTAL SECTION

Synthesis of SPG. SPG synthesis was performed using a commercially available Panasonic INVERTER 1200 W microwave oven. A mixture of 0.05 g (4.17 mmol) of AF-MWCNTs, 1.50 g (10.13 mmol) of *O*-phthalic anhydride acid, 2.50 g (41.7 mmol) of urea, 1.25 g (4.75 mmol) of $CoCl_2{\cdot}6H_2O$, 2.50 g (46.75 mmol) of NH_4Cl, and 0.10 g (0.08 mmol) of $(NH_4)_6Mo_7O_{24}{\cdot}4H_2O$ was mechanically ground and transferred to a 150 mL crucible. The crucible was then irradiated in a microwave oven at 600 W for 10 min and subsequently at 800 W for 10 min. The postmicrowaved product was immediately quenched using ice water. The quench aided in the exfoliation of the material to make thin nonrestacking graphene flakes. It was then thoroughly rinsed with several iterations of water, acetone, and alcohol and dried under vacuum at 70 °C overnight. The purification of the as-products was done by using 100 mL of 2 mol L^{-1} hydrochloric acid to remove metal particles, followed by rinsing with hot water several times to remove the residues such as $(NH_4)_2Mo_2O_7$. Subsequently, the products were washed by ethanol three times. The precipitate was finally dried out under vacuum at 70 °C overnight. The final yield was 0.67 g, with the initial 0.05 g of AF-MWCNTs making up ∼7.5 wt % of the material. A reference graphite/MWCNTs composite was prepared by using an identical synthesis process and precursors as the SPG, but without the final quenching step. Rather, the samples were allowed to air cool after microwave heating. A reference CoPc−MWCNT composite was also prepared by microwave synthesis (details are shown in the Supporting Information).

Reference two-dimensional graphene nanoflakes (labeled 2D) were purchased from cheaptubes.com and were utilized without any additional modification. The flakes were "Grade 3" reduced graphene nanoflakes, being 4−5 layers (around 8 nm thick) on average with typical particle diameters of less than 2 μm. A representative SEM micrograph of the commercial two-dimensional graphene nanoflakes is shown in Supporting Information, Figure S12.

Characterization. The SEM images of the samples were obtained with a Hitachi S-4800 scanning electron microscope equipped with a field emission gun. The TEM and the selected-area electron diffraction (SAED) of the samples were performed on a field emission transmission electron microscopy JEOL 2100 at 200 kV accelerating voltage. Raman spectroscopy was performed with a NICOLET AlMEGA XR dispersive Raman system utilizing a laser power of 532 nm−24 mV, resulting in an approximately 2 μm diameter sampling cross section. The XPS spectra were recorded on an Axis Ultra spectrometer with an Al (Mono) Kα X-ray source (1486.6 eV). The base pressure of the analysis chamber was below 10^{-9} mbar. For the surface area analysis, the porous texture of the obtained material was characterized by nitrogen adsorption at 77 K (Quantachrome Autosorb-1). Thermal gravimetric analysis and differential scanning calorimetry analysis (TGA/DSC) were performed on a SDT Q600, TA Instruments DSC/TGA, in air with a heating rate of 10 °C min^{-1}.

Electrochemistry. For electrochemical tests in aqueous electrolyte, a slurry containing 85% of the obtained products, 10% carbon black, and 5% binder (PVDF) suspended in *N*-methylpyrrolidone was coated on a glassy carbon disk (1 cm^2) and then dried at 110 °C overnight in a vacuum oven. The carbon disk was then sealed in a Teflon electrode assembly using epoxy resin. The electrochemical experiments were performed in Teflon beakers in 1 M H_2SO_4 using two pieces of electrodes with identical mass loading (around 2 mg on each side). Pt wire and Ag/AgCl (1 M KCl) were used as the counter electrode and reference electrode for the three-electrode setup. For electrochemical tests in an IL, the slurry was coated on a stainless disk instead of a glassy carbon disk and dried under the same conditions. Two symmetrical electrodes separated by a porous polymeric separator were sealed in a 2032 stainless steel coin cell filled with BMPY TFSI (>98%, Ionic Liquids Technologies Inc., U.S.A.). The cyclic voltammetry and galvanostatic charge−discharge cycling were performed on a Solartron 1470E Multichannel Potentiostat/Cell Test System. The energy density and the power density were calculated using a two-electrode setup; energy density = $1/2C_{cell}V^2$ and power density = $IV/(2m)$, where I is the change/discharge current, m is the mass of the active material per electrode, and V is the potential window after the deduction of the IR drop. The material-specific capacitance (C_{mater}) was back calculated from the two-electrode cell-specific capacitance (C_{cell}) by the following relation: $C_{mater} = 4C_{cell} = 4It/(2mV) = 2It/(mV)$, where t is the discharging time.

ASSOCIATED CONTENT

Supporting Information

Formation of CoPc−MWCNTs and graphite−MWCNTs, XPS spectra of AF-MWCNTs and the SPG, XRD pattern of AF-MWCNTs and detailed X-ray analysis procedure, thermal analysis, CV curves of 3D SPG in a three-electrode system, and capacitance retention of 3D SPG versus the cycle number in an IL. This material is available free of charge via the Internet at http://pubs.acs.org.

AUTHOR INFORMATION

Corresponding Author

*E-mail: lizhicn@gmail.com (Z.L.); dmitlin@ualberta.ca (D.M.).

Author Contributions

[§]These authors contributed to this work equally

Notes

The authors declare no competing financial interest.

ACKNOWLEDGMENTS

This work was funded by NSERC Discovery, NINT NRC, and University of Alberta nanoBridge.

REFERENCES

(1) Zhu, Y. W.; Murali, S.; Stoller, M. D.; Ganesh, K. J.; Cai, W. W.; Ferreira, P. J.; Pirkle, A.; Wallace, R. M.; Cychosz, K. A.; Thommes, M.; et al. Carbon-Based Supercapacitors Produced by Activation of Graphene. *Science* **2011**, *332*, 1537−1541.

(2) Liu, C. G.; Yu, Z. N.; Neff, D.; Zhamu, A.; Jang, B. Z. Graphene-Based Supercapacitor with an Ultrahigh Energy Density. *Nano Lett.* **2010**, *10*, 4863−4868.

(3) Chu, A.; Braatz, P. Comparison of Commercial Supercapacitors and High-Power Lithium-Ion Batteries for Power-Assist Applications

in Hybrid Electric Vehicles I. Initial Characterization. *J. Power Sources* **2002**, *112*, 236−246.
(4) Li, Z.; Zhang, L.; Amirkhiz, B. S.; Tan, X. H.; Xu, Z. W.; Wang, H. L.; Olsen, B. C.; Holt, C. M. B.; Mitlin, D. Carbonized Chicken Eggshell Membranes with 3D Architectures as High-Performance Electrode Materials for Supercapacitors. *Adv. Energy Mater.* **2012**, *2*, 431−437.
(5) Kim, T. Y.; Lee, H. W.; Stoller, M.; Dreyer, D. R.; Bielawski, C. W.; Ruoff, R. S.; Suh, K. S. High-Performance Supercapacitors Based on Poly(ionic liquid)-Modified Graphene Electrodes. *ACS Nano* **2011**, *5*, 436−442.
(6) Jasuja, K.; Linn, J.; Melton, S.; Berry, V. Microwave-Reduced Uncapped Metal Nanoparticles on Graphene: Tuning Catalytic, Electrical, and Raman Properties. *J. Phys. Chem. Lett.* **2010**, *1*, 1853−1860.
(7) Jang, I. Y.; Ogata, H.; Park, K. C.; Lee, S. H.; Park, J. S.; Jung, Y. C.; Kim, Y. J.; Kim, Y. A.; Endo, M. Exposed Edge Planes of Cup-Stacked Carbon Nanotubes for an Electrochemical Capacitor. *J. Phys. Chem. Lett.* **2010**, *1*, 2099−2103.
(8) Wang, Y. H.; Zhitomirsky, I. Electrophoretic Deposition of Manganese Dioxide−Multiwalled Carbon Nanotube Composites for Electrochemical Supercapacitors. *Langmuir* **2009**, *25*, 9684−9689.
(9) Miller, J. R.; Outlaw, R. A.; Holloway, B. C. Graphene Double-Layer Capacitor with ac Line-Filtering Performance. *Science* **2010**, *329*, 1637−1639.
(10) Zhu, Y. W.; Murali, S.; Stoller, M. D.; Velamakanni, A.; Piner, R. D.; Ruoff, R. S. Microwave Assisted Exfoliation and Reduction of Graphite Oxide for Ultracapacitors. *Carbon* **2010**, *48*, 2118−2122.
(11) Guo, S. J.; Dong, S. J. Graphene Nanosheet: Synthesis, Molecular Engineering, Thin Film, Hybrids, and Energy and Analytical Applications. *Chem. Soc. Rev.* **2011**, *40*, 2644−2672.
(12) Conway, B. E. *Electrochemical Supercapacitors, Scientific Fundamentals and Technological Applications*; Kluwer Academic/Plenum: New York, 1999.
(13) Yang, X. W.; Zhu, J. W.; Qiu, L.; Li, D. Bioinspired Effective Prevention of Restacking in Multilayered Graphene Films: Towards the Next Generation of High-Performance Supercapacitors. *Adv. Mater.* **2011**, *23*, 2833−2838.
(14) El-Kady, M. F.; Strong, V.; Dubin, S.; Kaner, R. B. Laser Scribing of High-Performance and Flexible Graphene-Based Electrochemical Capacitors. *Science* **2012**, *335*, 1326−1330.
(15) Dimitrakakis, G. K.; Tylianakis, E.; Froudakis, G. E. Pillared Graphene: A New 3-D Network Nanostructure for Enhanced Hydrogen Storage. *Nano Lett.* **2008**, *8*, 3166−3170.
(16) Zhang, L. L.; Xiong, Z. G.; Zhao, X. S. Pillaring Chemically Exfoliated Graphene Oxide with Carbon Nanotubes for Photocatalytic Degradation of Dyes under Visible Light Irradiation. *ACS Nano* **2010**, *4*, 7030−7036.
(17) Lee, S. H.; Kim, H. W.; Hwang, J. O.; Lee, W. J.; Kwon, J.; Bielawski, C. W.; Ruoff, R. S.; Kim, S. O. Three-Dimensional Self-Assembly of Graphene Oxide Platelets into Mechanically Flexible Macroporous Carbon Films. *Angew. Chem., Int. Ed.* **2010**, *49*, 10084−10088.
(18) Chen, Z. P.; Ren, W. C.; Gao, L. B.; Liu, B. L.; Pei, S. F.; Cheng, H. M. Three-Dimensional Flexible and Conductive Interconnected Graphene Networks Grown by Chemical Vapour Deposition. *Nat. Mater.* **2011**, *10*, 424−428.
(19) Tylianakis, E.; Psofogiannakis, G. M.; Froudakis, G. E. Li-Doped Pillared Graphene Oxide: A Graphene-Based Nanostructured Material for Hydrogen Storage. *J. Phys. Chem. Lett.* **2010**, *1*, 2459−2464.
(20) Xu, Y. X.; Sheng, K. X.; Li, C.; Shi, G. Q. Self-Assembled Graphene Hydrogel via a One-Step Hydrothermal Process. *ACS Nano* **2010**, *4*, 4324−4330.
(21) Jhung, S. H.; Jin, T. H.; Hwang, Y. K.; Chang, J. S. Microwave Effect in the Fast Synthesis of Microporous Materials: Which Stage between Nucleation and Crystal Growth is Accelerated by Microwave Irradiation? *Chem.—Eur. J.* **2007**, *13*, 4410−4417.
(22) Guo, S. J.; Wen, D.; Zhai, Y. M.; Dong, S. J.; Wang, E. K. Platinum Nanoparticle Ensemble-on-Graphene Hybrid Nanosheet: One-Pot, Rapid Synthesis, and Used as New Electrode Material for Electrochemical Sensing. *Acs Nano* **2010**, *4*, 3959−3968.
(23) Economopoulos, S. P.; Rotas, G.; Miyata, Y.; Shinohara, H.; Tagmatarchis, N. Exfoliation and Chemical Modification Using Microwave Irradiation Affording Highly Functionalized Graphene. *ACS Nano* **2010**, *4*, 7499−7507.
(24) Tu, W. G.; Zhou, Y.; Liu, Q.; Tian, Z. P.; Gao, J.; Chen, X. Y.; Zhang, H. T.; Liu, J. G.; Zou, Z. G. Robust Hollow Spheres Consisting of Alternating Titania Nanosheets and Graphene Nanosheets with High Photocatalytic Activity for CO_2 Conversion into Renewable Fuels. *Adv. Funct. Mater.* **2012**, *22*, 1215−1221.
(25) Xu, Z. W.; Li, H. J.; Li, W.; Cao, G. X.; Zhang, Q. L.; Li, K. Z.; Fu, Q. G.; Wang, J. Large-Scale Production of Graphene by Microwave Synthesis and Rapid Cooling. *Chem. Commun.* **2011**, *47*, 1166−1168.
(26) Lever, A. B. P. The Phthalocyanines — Molecules of Enduring Value; A Two-Dimensional Analysis of Redox Potentials. *J. Porphyrins Phthalocyanines* **1999**, *3*, 488−499.
(27) Scheidt, W. R.; Dow, W. Molecular Stereochemistry of Phthalocyanatozinc(II). *J. Am. Chem. Soc.* **1977**, *99*, 1101−1104.
(28) Leznoff, C. C.; Black, L. S.; Hiebert, A.; Causey, P. W.; Christendat, D.; Lever, A. B. P. Red Manganese Phthalocyanines from Highly Hindered Hexadecaalkoxyphthalocyanines. *Inorg. Chim. Acta* **2006**, *359*, 2690−2699.
(29) Lin, R. Y.; Taberna, P. L.; Fantini, S.; Presser, V.; Perez, C. R.; Malbosc, F.; Rupesinghe, N. L.; Teo, K. B. K.; Gogotsi, Y.; Simon, P. Capacitive Energy Storage from −50 to 100 °C Using an Ionic Liquid Electrolyte. *J. Phys. Chem. Lett.* **2011**, *2*, 2396−2401.
(30) Li, H. J.; Xu, Z. W.; Li, K. Z.; Hou, X. H.; Cao, G. X.; Zhang, Q. L.; Cao, Z. Y. Modification of Multiwalled Carbon Nanotubes with Cobalt Phthalocyanine: Effects of the Templates on The assemblies. *J. Mater. Chem.* **2011**, *21*, 1181−1186.
(31) Yan, J.; Liu, J. P.; Fan, Z. J.; Wei, T.; Zhang, L. J. High-Performance Supercapacitor Electrodes Based on Highly Corrugated Graphene Sheets. *Carbon* **2012**, *50*, 2179−2188.
(32) Gong, K. P.; Du, F.; Xia, Z. H.; Durstock, M.; Dai, L. M. Nitrogen-Doped Carbon Nanotube Arrays with High Electrocatalytic Activity for Oxygen Reduction. *Science* **2009**, *323*, 760−764.
(33) Ferrari, A. C.; Meyer, J. C.; Scardaci, V.; Casiraghi, C.; Lazzeri, M.; Mauri, F.; Piscanec, S.; Jiang, D.; Novoselov, K. S.; Roth, S.; et al. Raman Spectrum of Graphene and Graphene Layers. *Phys. Rev. Lett.* **2006**, *97*, 187401.
(34) Magasinski, A.; Dixon, P.; Hertzberg, B.; Kvit, A.; Ayala, J.; Yushin, G. High-Performance Lithium-Ion Anodes Using a Hierarchical Bottom-Up Approach. *Nat. Mater.* **2010**, *9*, 353−358.
(35) Hulicova-Jurcakova, D.; Seredych, M.; Lu, G. Q.; Bandosz, T. J. Combined Effect of Nitrogen- and Oxygen-Containing Functional Groups of Microporous Activated Carbon on its Electrochemical Performance in Supercapacitors. *Adv. Funct. Mater.* **2009**, *19*, 438−447.
(36) Largeot, C.; Portet, C.; Chmiola, J.; Taberna, P. L.; Gogotsi, Y.; Simon, P. Relation Between the Ion Size and Pore Size for an Electric Double-Layer Capacitor. *J. Am. Chem. Soc.* **2008**, *130*, 2730−2731.
(37) Sillars, F. B.; Fletcher, S. I.; Mirzaeian, M.; Hall, P. J. Effect of Activated Carbon Xerogel Pore Size on the Capacitance Performance of Ionic Liquid Electrolytes. *Energ. Environ. Sci.* **2011**, *4*, 695−706.
(38) Largeot, C.; Taberna, P. L.; Gogotsi, Y.; Simon, P. Microporous Carbon-Based Electrical Double Layer Capacitor Operating at High Temperature in Ionic Liquid Electrolyte. *Electrochem. Solid St.* **2011**, *14*, A174−A176.
(39) Gamby, J.; Taberna, P. L.; Simon, P.; Fauvarque, J. F.; Chesneau, M. Studies and Characterizations of Various Activated Carbons Used for Carbon/Carbon supercapacitors. *J. Power Sources* **2001**, *101*, 109−116.